

Forecasting density-valued functional panel data

Cristian F. Jiménez-Varón *

Department of Mathematics

University of York

Department of Physics and Mathematics

Universidad Autónoma de Manizales

Ying Sun 

CEMSE Division, Statistics Program

King Abdullah University of Science and Technology

Han Lin Shang 

Department of Actuarial Studies and Business Analytics

Macquarie University

Abstract

We introduce a statistical method for modeling and forecasting functional panel data represented by multiple densities. Density functions are nonnegative and have a constrained integral and thus do not constitute a linear vector space. We implement a center log-ratio transformation to transform densities into unconstrained functions. These functions exhibit cross-sectional correlation and temporal dependence. Via a functional analysis of variance decomposition, we decompose the unconstrained functional panel data into a deterministic trend component and a time-varying residual component. To produce forecasts for the time-varying component, a functional time series forecasting method, based on the estimation of the long-run covariance, is implemented. By combining the forecasts of the time-varying residual component with the deterministic trend component, we obtain h -step-ahead forecast curves for multiple populations. Illustrated by age- and sex-specific life-table death counts in the United States, we apply our proposed method to generate forecasts of the life-table death counts for 51 states.

Keywords: Compositional data analysis; Constrained functional time series; Density function forecasting; Functional median polish; Functional two-way analysis of variance

*Postal address: Department of Mathematics. University of York, Heslington, York YO10 5DD, United Kingdom.
E-mail: cristian.jimenezvaron@york.ac.uk

1 Introduction

Actuaries and demographers are interested in developing models for mortality forecasting (see, e.g., [Basellini et al., 2023](#), for comprehensive reviews). From an actuary perspective, mortality forecasts are important inputs in pricing fixed-term or lifetime annuities and setting of reserves. They are important to manage the financial effects of mortality improvements over time on pensions and are essential to the financial viability of life insurance companies. From a demography perspective, mortality forecasts are essential to health-care and aged-care systems and are an important component of population forecasts for urban and rural planning.

For modeling age-specific mortality, three functions related to mortality are commonly studied: mortality rate, survival function, and life-table death counts. Mortality rates are bounded between 0 and 1. The survival function monotonically decreases. The life-table death counts of each age group are non-negative and sum to a radix of 10^5 each year, which strongly resembles probability density functions (PDFs). Among these three functions, life-table death counts provide important insights into longevity risk and lifespan variability that cannot be easily quantified from either hazard or survival function. These additional constraints on the life-table death counts can be helpful to improve forecast accuracy (see, e.g., [Oeppen, 2008](#)). For instance, in many developed countries, deaths at younger ages gradually shift toward older ages. In addition to providing an informative description of the mortality experience of a population, the life-table death counts yield readily available information on "central longevity indicators", that is, mean, median, and mode age at death ([Canudas-Romo, 2010](#)), and lifespan variability ([Robine, 2001](#)). For many developed countries, a decrease in variability over time may be observed through the Gini coefficient of life-table ages at death (see, e.g., [Shang et al., 2022](#)) or Drewnowski's index (see, e.g., [Aburto et al., 2022](#)).

Because of the two constraints, life-table death counts can be viewed as compositional data. Compositional data are defined as a random vector of D compositions $[d_1, d_2, \dots, d_D]$, non-negative values in which the sum of is a given constant, typically one (portions) in PDF, 100 (%) in weekly household expenditure (see, e.g., [Scealy and Welsh, 2017](#)), and 10^6 for parts per million in geochemical compositions (see, e.g., [Scealy et al., 2015](#)). The sample space of compositional data is a (nonlinear) simplex

$$\mathcal{S}^D = \left\{ (d_1, d_2, \dots, d_D)^\top, \quad d_x > 0, \quad \sum_{x=1}^D d_x = c \right\}, \quad (1)$$

where d_x denotes life-table death count for age x , where $x = 1, 2, \dots, D$ and D denotes the total

number of discrete ages, c is a fixed constant, and \top denotes vector transpose.

In compositional data analysis, there exist several transformations from the simplex to Euclidean space. Among them, the center log-ratio (clr) is the simplest and most widely used transformation because principal component analysis (PCA) is not invariant to a permutation of the compositions (Aitchison, 1982). For a given year t , the clr transformation is defined as

$$\begin{aligned} y_{t,x} &= \ln \left\{ \frac{d_{t,x}}{(\prod_{x=1}^D d_{t,x})^{1/D}} \right\}, \\ &= \ln d_{t,x} - \frac{1}{D} \sum_{x=1}^D \ln d_{t,x}, \end{aligned} \quad (2)$$

where $\ln(\cdot)$ denotes natural logarithm, $\mathbf{y}_t = (y_{t,1}, y_{t,2}, \dots, y_{t,D})^\top$ for $t = 1, 2, \dots, T$. From a time series of $\mathbf{Y} = (\mathbf{y}_1, \mathbf{y}_2, \dots, \mathbf{y}_T)$, Bergeron-Boucher et al. (2017) applied a principal component analysis (PCA) to extract latent principal components and their associated scores. The scores can be modeled and forecast using a univariate time series forecasting method. With the forecast principal component scores, $\hat{\mathbf{y}}_{T+h|T}$ can be obtained with the estimated principal components. By taking the inverse clr transformation, $\mathbf{d}_{T+h|T}$ can be estimated by

$$\hat{\mathbf{d}}_{T+h|T} = \frac{\exp(\hat{\mathbf{y}}_{T+h|T,x})}{\sum_{x=1}^D \exp(\hat{\mathbf{y}}_{T+h|T,x})} \times 10^5,$$

where 10^5 is the radix reported in the Human Mortality Database (2024).

Extending these works, our contribution is to develop statistical models to jointly forecast life-table death counts as a function of age at the *sub-national* level. Understanding patterns in mortality across subpopulations is essential for local health policy decision-making, identifying mortality patterns of vulnerable groups, classifying heterogeneous populations into homogeneous groups, and tracking the effects of policy responses. The series at the sub-national level presents two challenges: (1) the signal-to-noise ratio is comparably low; and (2) the number of series may exceed the number of curves in a series. The latter leads to the study of high-dimensional functional time series (HDFTS) (see, e.g., Gao et al., 2019; Jiménez-Varón et al., 2024; Chang et al., 2025).

In the context of HDFTS, Zhou and Dette (2023) derived Gaussian and multiplier bootstrap approximations for sums of HDFTS. These approximations were utilized to construct joint simultaneous confidence bands for the mean functions and develop a hypothesis test to assess the parallel behavior of the mean functions in the panel dimension. Hallin et al. (2023) investigated the representation of HDFTS using a factor model, identifying crucial conditions on the eigenvalues

of the covariance operator for the existence and uniqueness of the factor model. [Gao et al. \(2019\)](#) adopted a two-stage approach, combining truncated principal component analysis and a separate scalar factor model for the resulting panels of scores. In contrast, [Tavakoli et al. \(2023\)](#) introduced a functional factor model with a functional factor loading and a vector of real-valued factors, while [Guo et al. \(2024\)](#) considered a functional factor model with a real-valued factor loading and a functional factor. Additionally, [Tang et al. \(2022\)](#) studied clustering problems for age-specific mortality rates as an example of HDFTS, and [Li et al. \(2024\)](#) proposed hypothesis tests for detecting and identifying change points, and clustering of change points in HDFTS using an information criterion.

In the realm of estimating HDFTS models, [Guo and Qiao \(2023\)](#) introduced a three-step procedure that incorporates a novel functional stability measure, the non-asymptotic properties of functional principal component analysis (FPCA), and a regularization approach for estimating autoregressive coefficients. Moreover, [Tan et al. \(2024\)](#) proposed dynamic weak separability to characterize the two-way dependence structure in multivariate functional time series, developing a unified framework for functional graphical models and dynamic principal component analysis. [Chang et al. \(2024\)](#) presented a three-step framework for statistical learning of HDFTS with errors, incorporating autocovariance-based dimension reduction and a novel block regularized minimum distance estimation.

In practice, it is common to find functional objects that do not reside in a linear Hilbert space. This is exemplified by various scenarios, such as analyzing time series consisting of PDFs and cumulative density functions (CDFs). In the context of PDFs, the works of [Pascariu et al. \(2019\)](#) and [Shang et al. \(2022\)](#) have studied the age distribution of death counts. In particular, [Shang et al. \(2022\)](#) have proposed a forecasting method that utilizes the location and shape measures of density functions. Moreover, in nonstationary time series, [Chang et al. \(2016\)](#) have considered modeling state densities, while [Horta and Ziegelmann \(2018\)](#) have explored the dynamics of financial return densities. In terms of CDFs, [Condino \(2023\)](#) have examined a sequence of Lorenz curves derived from a regional household income and wealth survey in Italy. [Zhang et al. \(2024\)](#) proposed a functional ridge-regression-based estimation method that estimates CDFs accurately. We aim to introduce a forecasting method for HDFTS where the functional objects are PDFs.

When the functional objects are nonlinear, it is common to transform the functional objects into a linear space. A popular space is the Bayes Hilbert space studied in [Hron et al. \(2016\)](#). [Hron et al. \(2016\)](#) introduced the simplicial FPCA of densities. Simplicial FPCA is based on the geometry of

the Bayes space of functional compositions. It utilizes the clr transformation to map the densities to a suitable Hilbert space, enabling the application of standard functional data analytic techniques. [Seo and Beare \(2019\)](#) focused on modeling nonstationary time series of PDFs. They illustrated the isomorphism between a cointegrated Bayes Hilbert space and a cointegrated linear process in a Hilbert space of centered square-integrable real functions.

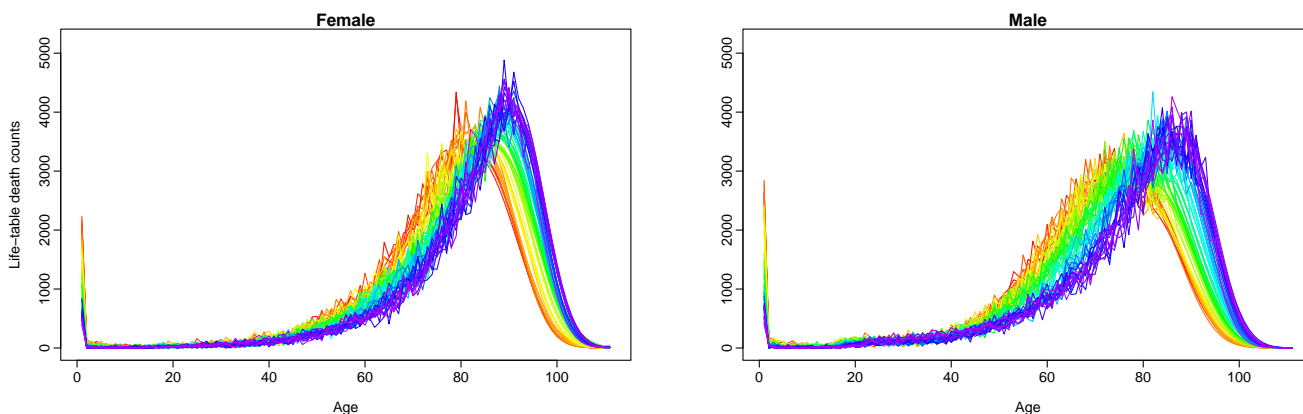
A unique feature associated with the HDFTS is that they can be cross-sectionally correlated and temporally dependent. We deploy a two-way functional analysis of variance (ANOVA), as used by [Jiménez-Varón et al. \(2024\)](#) to decompose HDFTS into a deterministic trend component and a residual component that varies over time. These components can be estimated by functional median polish decomposition (FMP-ANOVA) and functional analysis of variance based on means (FM-ANOVA). Both decompositions compute the functional grand effect and functional main factor effects in an additive model without factor interaction. The FM-ANOVA has been extensively studied by [Zhang \(2014\)](#). The FMP-ANOVA was proposed by [Sun and Genton \(2012\)](#) as an extension of the univariate median polish of [Tukey \(1977\)](#). It is a robust statistical technique for studying the effects of factors on the response since it replaces the mean with the median. Our proposed functional time series forecasting method for densities is then compared with existing methods, such as the factor models from [Gao et al. \(2019\)](#) and [Tavakoli et al. \(2023\)](#), and the maximum entropy mortality model proposed by [Pascariu et al. \(2019\)](#).

The remainder of this paper is structured as follows. In Section 2, we present the United States (US) sub-national mortality rates across 51 states. In Section 3, we apply functional ANOVA decomposition to extract a deterministic trend component and a time-varying residual component. For modeling and forecasting the residual component, we introduce a functional time series forecasting method based on FPCA for producing forecasts. By combining the time-varying component forecasts with the deterministic component, we obtain h -step-ahead forecast curves for multiple populations. With the inverse clr transformation, we transform our forecast curves back to the simplex. In doing so, we obtain forecast life-table death counts. We evaluate and compare point forecast accuracies in Section 4. Section 5 concludes and offers some ideas on how the methodology presented can be further extended.

2 Age distribution of life-table death counts in the United States

We consider US age- and sex-specific life-table death counts from 1959 to 2020, obtained from the [United States Mortality Database \(2024\)](#). The database documents a historical set of complete state-level life tables designed to foster research on geographic variations in mortality across the US and monitor trends in health inequalities. This data set includes complete and abridged life tables by sex for each of the nine Census Divisions, four Census Regions, 50 States of the US, as well as the District of Columbia, with mortality up to age 110.

The life-table radix is fixed at 10^5 at age 0 for each year. For the life-table death counts, there are 111 ages, and these are age 0, 1, ..., 109, 110+. Due to rounding, there may be zero counts, especially for older ages at some years. To rectify the problem, one can also use the probability of dying (i.e., q_x) and the life-table radix to recalculate the estimated death counts with decimal places. The smoother estimates are more detailed than those reported in the [United States Mortality Database \(2024\)](#).



(a) Rhode Island data series between 1959 and 2020

(b) Rhode Island data series between 1959 and 2020

Figure 1: Rainbow plots of age-specific life-table death count from 1959 to 2020 in a single-year group in Rhode Island, US. The oldest years are shown in red, with the most recent in violet. Curves are ordered chronologically according to the colors of the rainbow.

To understand the primary features of the data, Figures 1a and 1b present rainbow plots of the female and male age-specific life-table death counts in Rhode Island in a single-year group, respectively. The time ordering of the curves follows the colors of the rainbow, where data from the distant past are shown in red and more recent data are shown in purple. Both figures demonstrate a decreasing trend in infant mortality and a negatively skewed distribution for the life-table death counts, where the peaks shift to older ages for both females and males. The shift of the distribution symbolizes longevity risk, which can be a major issue for insurers and government pensions,

especially in the selling and risk management of annuities (see [Brouhns et al., 2002](#); [Canudas-Romo, 2010](#), for discussion).

To measure the spread of the distribution, we consider the Gini coefficient. It is a measure that quantifies the level of inequality in age at death within a life table population. A lower Gini coefficient value indicates less age variability at death, suggesting a greater level of equality ([Basellini et al., 2020](#); [Aburto et al., 2022](#)). In Figure 2, we present the Gini coefficient for the US for the female population (left) and male population (right). We can observe from both figures that, on average, there has been an increasing trend in the Gini coefficient over the years. The observed increasing tendency can be explained by a continuous decrease in the ratio between the resulting life expectancy at birth when doubling the hazard at all ages and the overall life expectancy at birth ([Aburto et al., 2022](#)).

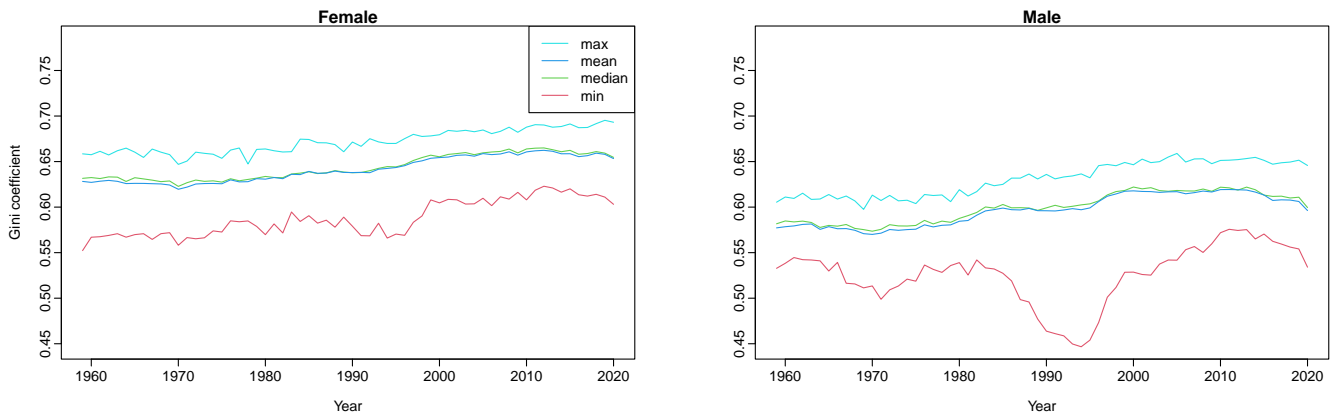


Figure 2: Summary statistics (maximum, mean, median, and minimum) for the Gini coefficients in the US aggregated across the 51 states.

3 Methodology

The life-table death counts are discrete and densely observed. By adopting the linear interpolation, we convert them into a continuous function on the same function support $u \in (x_1, x_D)$, where x_1 and x_D represent the first and last age groups, respectively.

3.1 Center log-ratio transformation for density-valued functional time series

Let $d_{t,s}^g(u)$ be the age-specific life-table death count for age u , state s , gender g at year t . For a given year t , compositional data are defined as a random vector of non-negative components, and the sum of which is a specified constant. Between the non-negativity and summability constraints, the

sample space of functional compositional data is a simplex of the form in (1).

When age $u \in [x_1, x_D]$ is treated as a continuum, the clr transformation in (2) can be written as

$$\text{clr}[d_{t,s}^g(u)] := \mathcal{Y}_{t,s}^g(u) = \ln d_{t,s}^g(u) - \frac{1}{\eta} \int_{x_1}^{x_D} \ln d_{t,s}^g(u) du,$$

where $\eta = x_D - x_1$ denotes the length of the age interval, and $\frac{1}{\eta} \int_{x_1}^{x_D} \ln d_{t,s}^g(u) du$ is the geometric mean. Let $\mathcal{Y}_{t,s}^g(u)$ be the transformed data for age u , state s , gender g at year t . When considering life-table death counts as density curves, [Shang and Haberman \(2020\)](#) and [Shang et al. \(2022\)](#) developed a functional principal component regression to forecast a time series of density curves in the constrained space. Via the inverse clr transformation, the forecast life-table death counts can be obtained as

$$\hat{d}_{T+h|T,s}^g(u) = \frac{\exp[\hat{\mathcal{Y}}_{T+h|T,s}^g(u)]}{\int_{x_1}^{x_D} \exp[\hat{\mathcal{Y}}_{T+h|T,s}^g(u)] du} \times 10^5.$$

3.2 Two-way functional ANOVA model

By treating age u as a continuum, a two-way functional ANOVA decomposition can be expressed as:

$$\mathcal{Y}_{t,s}^g(u) = \underbrace{\mu(u) + \alpha_s(u) + \beta^g(u)}_{\text{Deterministic} := \mathcal{D}_s^g(u)} + \underbrace{\mathcal{X}_{t,s}^g(u)}_{\text{time-varying}}, \quad u \in \mathcal{I} \subset \mathcal{R}. \quad (3)$$

where $\mu(u)$ denotes the functional grand effect, $\alpha_s(u)$ denotes the functional row effect, and, $\beta^g(u)$ denotes the functional column effect. For each state s and gender g , we considered replicates for the years t with time horizon, for $t = 1, 2, \dots, T$, $s = 1, 2, \dots, n_s$, and $g = \{\text{Female(F), Male(M)}\}$. $\mathcal{X}_s^g(u) = [\mathcal{X}_{1,s}^g(u), \dots, \mathcal{X}_{T,s}^g(u)]$ denotes the residual component that varies over time for the state s and gender g . Such a decomposition is not an approximation and can exactly reconstruct the original data.

The model described in (3), can be estimated in two ways: the FM-ANOVA approach ([Zhang, 2014](#); [Ramsay and Silverman, 2006](#)) or FMP-ANOVA approach ([Sun and Genton, 2012](#)). The former extracts the deterministic component into the following terms:

$$\begin{aligned} \hat{\mu}(u) &= \frac{1}{n_s \times 2 \times T} \sum_{s=1}^{n_s} \sum_{g=1}^2 \sum_{t=1}^T \mathcal{Y}_{t,s}^g(u) \\ \hat{\alpha}_s(u) &= \frac{1}{2 \times T} \sum_{g=1}^2 \sum_{t=1}^T \mathcal{Y}_{t,s}^g(u) - \hat{\mu}(u) \\ \hat{\beta}^g(u) &= \frac{1}{n_s \times T} \sum_{s=1}^{n_s} \sum_{t=1}^T \mathcal{Y}_{t,s}^g(u) - \hat{\mu}(u). \end{aligned}$$

There exist some identifiability constraints, so that for all $u \in \mathcal{I}$, $\sum_{s=1}^{n_s} \alpha_s(u) = \sum_{g=1}^2 \beta^g(u) = 0$, and $\sum_{s=1}^{n_s} \mathcal{X}_{t,s}^g(u) = \sum_{g=1}^2 \mathcal{X}_{t,s}^g(u) = 0$ for all t (Ramsay and Silverman, 2006, Chapter 13). The FMP-ANOVA decomposition satisfies that $\forall u \in \mathcal{I}$, $\text{median}_s\{\alpha_s(u)\} = 0$, $\text{median}_g\{\beta^g(u)\} = 0$, $\text{median}_s\{\mathcal{X}_{t,s}^g(u)\} = \text{median}_g\{\mathcal{X}_{t,s}^g(u)\} = 0$ for all t (Sun and Genton, 2012).

3.3 Point forecasts based on functional analysis of variance

For the functional residual process obtained from either the FMP-ANOVA or FM-ANOVA, we consider a functional time series forecasting method based on the FPCA of Shang (2019). The proposed FPCA relies on an accurate estimate of the long-run covariance function, for which we consider a kernel sandwich estimator with plug-in bandwidth (see, e.g., Horváth et al., 2016; Rice and Shang, 2017).

For a given state s and gender g , denote $\mathcal{X}_{t,s}^g(u)$ as a stationary ergodic functional time series exhibiting stationarity and ergodicity. In essence, the statistical features of a stochastic process will not vary over time, and they can be obtained from a single, sufficiently long sample of the process. For such a random process, the long-run covariance function can be defined as

$$\begin{aligned} C_s^g(u, v) &= \sum_{l=-\infty}^{\infty} \gamma_{l,s}^g(u, v) \\ &= \sum_{l=-\infty}^{\infty} \text{cov}[\mathcal{X}_{0,s}^g(u), \mathcal{X}_{l,s}^g(v)], \end{aligned}$$

where $u, v \in \mathcal{I}$ and l denote a lag variable.

While the long-run covariance can be expressed as a bi-infinite summation, its estimation is not trivial. For a finite sample, a natural estimator of $C(u, v)$ is

$$\widehat{C}_{T,s}^g(u, v) = \frac{1}{T} \sum_{|l|=0}^{|l| \leq T} (T - |l|) \widehat{\gamma}_{l,s}^g(u, v), \quad (4)$$

where $\overline{\mathcal{X}}_s^g = \frac{1}{T} \sum_{t=1}^T \mathcal{X}_{t,s}^g(u)$ and

$$\widehat{\gamma}_{l,s}^g(u, v) = \begin{cases} \frac{1}{T} \sum_{t=1}^{T-l} [\mathcal{X}_{t,s}^g(u) - \overline{\mathcal{X}}_s^g(u)] [\mathcal{X}_{t+l,s}^g(v) - \overline{\mathcal{X}}_s^g(v)] & \text{if } l \geq 0; \\ \frac{1}{T} \sum_{t=1-l}^T [\mathcal{X}_{t,s}^g(u) - \overline{\mathcal{X}}_s^g(v)] [\mathcal{X}_{t+l,s}^g(v) - \overline{\mathcal{X}}_s^g(v)] & \text{if } l < 0. \end{cases}$$

The long-run covariance function in (4) can be seen as a sum of autocovariance functions with decreasing weights. It is common in practice to determine the optimal lag value of l to balance the trade-off between squared bias and variance. In Li et al. (2020), l is the minimum between sample size T and the number of discretized points in a function. Other approaches use the kernel

sandwich estimator as in [Horváth et al. \(2016\)](#)

$$\widehat{\widehat{C}}_{T,b,s}^g(u,v) = \sum_{l=-\infty}^{\infty} W_q\left(\frac{l}{b}\right) \widehat{\gamma}_{l,s}^g(u,v),$$

where b is the bandwidth parameter, and $W_q(\cdot)$ is a symmetric weight function with bounded support of order q . [Rice and Shang \(2017\)](#) propose a plug-in algorithm for obtaining the optimal bandwidth parameter to minimize the asymptotic mean-squared normed error between the estimated and theoretical long-run covariance functions.

Via Mercer's lemma ([Mercer and Forsyth, 1909](#)), the estimated long-run covariance function $\widehat{\widehat{C}}_{T,b}^g(u,v)$ can be approximated by

$$\widehat{\widehat{C}}_{T,b,s}^g(u,v) = \sum_{k=1}^{\infty} \theta_k \phi_{k,s}^g(u) \phi_{k,s}^g(v),$$

where $\theta_1 \geq \theta_2 \geq \dots \geq 0$ are the eigenvalues of $\widehat{\widehat{C}}_{T,b,s}^g(u,v)$, and $[\phi_{1,s}^g(u), \phi_{2,s}^g(u), \dots]$ are the orthonormal functional principal components. We can project a functional time series onto a set of orthonormal functional principal components via the inner product in the corresponding Hilbert space. This leads to the Karhunen-Loève expansion of the realization of a stochastic process,

$$\begin{aligned} \mathcal{X}_{t,s}^g(u) &= \overline{\mathcal{X}}_s^g(u) + \sum_{k=1}^{\infty} \gamma_{k,t,s}^g \phi_{k,s}^g(u) \\ &= \overline{\mathcal{X}}_s^g(u) + \sum_{k=1}^K \gamma_{k,t,s}^g \phi_{k,s}^g(u) + \epsilon_{t,s}^g(u), \end{aligned}$$

where $\gamma_{k,t,s}^g = \langle \mathcal{X}_{t,s}^g(u) - \overline{\mathcal{X}}_s^g(u), \phi_{k,s}^g(u) \rangle$, denotes the k^{th} set of principal component scores for year t , sex s and geographical region g , and $\langle \cdot, \cdot \rangle$ denotes inner product. In addition, $\epsilon_{t,s}^g(u)$ denotes the error term with zero mean and finite variance, and K denotes the number of retained components.

There are various ways to determine the value of K : (1) scree plots or the fraction of variance explained by the first few functional principal components ([Chiou, 2012](#)); (2) pseudo-versions of Akaike information criterion and Bayesian information criterion ([Yao et al., 2005](#)); (3) predictive cross validation leaving out one or more curves ([Ramsay and Silverman, 2006](#)); (4) bootstrap methods ([Hall and Vial, 2006](#)); and (5) eigenvalue ratio criterion ([Ahn and Horenstein, 2013](#); [Li et al., 2021](#)). Here, we select K via the eigenvalue ratio criterion (EVR) of [Li et al. \(2021\)](#). The value of K is determined as the integer minimizing ratio of two adjacent empirical eigenvalues given by

$$\widehat{K} = \underset{1 \leq \kappa \leq \kappa_{\max}}{\operatorname{argmin}} \left\{ \frac{\widehat{\theta}_{\kappa+1}}{\widehat{\theta}_{\kappa}} \times \mathbb{1} \left(\frac{\widehat{\theta}_{\kappa+1}}{\widehat{\theta}_{\kappa}} \geq \delta \right) + \mathbb{1} \left(\frac{\widehat{\theta}_{\kappa+1}}{\widehat{\theta}_{\kappa}} \leq \delta \right) \right\}, \quad (5)$$

where δ is a pre-specified small positive number, set as $\delta = 1/\ln(\max\{\widehat{\theta}_1, T\})$, and $\mathbb{1}(\cdot)$ is the binary indicator function. κ_{\max} is a pre-specified positive integer, we choose κ_{\max} , as follows

$$\kappa_{\max} = \left| \left\{ \kappa \mid \widehat{\theta}_\kappa \geq \frac{1}{T} \sum_{\kappa=1}^T \widehat{\theta}_\kappa, \quad \kappa \geq 1 \right\} \right|,$$

where $|\cdot|$ denotes the cardinality of the set.

Because the female and male populations within a state can exhibit a strong dependence, we utilize a multivariate FPCA previously studied in [Shang and Kearney \(2022\)](#). For a given state s , collectively modeling multiple populations requires truncating K numbers of functional principal components of joint time series

$$\mathcal{X}_{t,s}(u) \approx \Phi_s(u) \Gamma_{t,s},$$

where $\mathcal{X}_{t,s}(u) = [\mathcal{X}_{t,s}^F(u), \mathcal{X}_{t,s}^M(u)]^\top$, superscripts ^F and ^M denote the female and male populations in a given state, and

$$\Gamma_{t,s} = \left[\gamma_{1,t,s}^F, \dots, \gamma_{K,t,s}^F, \gamma_{1,t,s}^M, \dots, \gamma_{K,t,s}^M \right]^\top,$$

is a $(2 \times K) \times 1$ vector of stacked principal component scores. $\Phi_s(u)$ is a $2 \times (2 \times K)$ matrix that contains the associated orthogonal basis functions. By conditioning on $\Phi_s(u)$, we obtain the h -step-ahead point forecasts as follows

$$\begin{aligned} \widehat{\mathcal{X}}_{T+h|T,s}(u) &= \mathbb{E} \left[\mathcal{X}_{T+h,s}(u) \mid \mathcal{X}_{1,s}(u), \dots, \mathcal{X}_{T,s}(u); \Phi_s(u) \right] \\ &= \overline{\mathcal{X}}_s(u) + \Phi_s(u) \widehat{\Gamma}_{T+h|T,s}, \end{aligned}$$

where $\overline{\mathcal{X}}_s(u) = [\overline{\mathcal{X}}_s^F(u), \overline{\mathcal{X}}_s^M(u)]$ represents the joint sample mean function.

A univariate time series method can be implemented to produce the forecasts of the principal component scores. The most commonly used methods are the exponential smoothing and autoregressive integrated moving average (ARIMA) models. For obtaining the forecast principal component score $\widehat{\Gamma}_{T+h|T,s}$, we apply the optimal ARIMA model selected by [Hyndman and Khandakar \(2008\)](#). Because the age-specific life-table death counts are observed yearly, the ARIMA takes the generic form of

$$(1 - \tau_1 \mathcal{B} - \dots - \tau_p \mathcal{B}^p) (1 - \mathcal{B})^d \gamma_\kappa = \psi + (1 + \nu_1 \mathcal{B} + \dots + \nu_q \mathcal{B}^q) \omega_\kappa, \quad (6)$$

where ψ represents the intercept, (τ_1, \dots, τ_p) denote the coefficients associated with the autoregressive component, γ_κ represents the principal component score, (ν_1, \dots, ν_q) denote the coefficients associated with the moving average component, \mathcal{B} denotes the backshift operator, $(1 - \mathcal{B})$ denotes the differencing operator, d represents the degree of integration, and ω_κ represents a white-noise

error term. The automatic selection method of [Hyndman and Khandakar \(2008\)](#) chooses the optimal autoregressive order p , moving average order q , and difference order d . The value of d is chosen using the Kwiatkowski-Phillips-Schmidt-Shin (KPSS) unit root tests ([Kwiatkowski et al., 1992](#)).

Once the forecasted functional residuals are obtained, we add the deterministic component from the FMP-ANOVA decomposition. As this is not time-varying, the overall h -step-ahead point forecast is defined as

$$\hat{\mathcal{Y}}_{T+h|T,s}^g(u) = \mathcal{D}_s^g(u) + \hat{\mathcal{X}}_{T+h|T,s}^g(u),$$

where $\mathcal{D}_s^g(u)$ is defined in (3). Then, we transform back to the original scale through the inverse clr transformation in Section 3.1.

4 Forecast accuracy evaluation of life-table death counts

We consider a rolling-window scheme to assess the point forecast as described in [Zivot and Wang \(2006, Chapter 9\)](#). The procedure is carried out as follows.

- 1) The transformed data are decomposed, through the two-way FMP-ANOVA and FM-ANOVA in Section 3.2, into deterministic and time-varying components. The two factors are the state s and gender g (males and females). The functional residual curves $[\mathcal{X}_{1,s}^g(u), \dots, \mathcal{X}_{T,s}^g(u)]$ are those obtained after removing all deterministic components.
- 2) We perform an h -step-ahead point forecast of the time-varying component. Then, we add the deterministic components to obtain the point forecast of the future curves.
- 3) To compute each of the h -step-ahead point forecasts, for $h = 1, 2, \dots, H$, we proceed as follows: we consider a rolling window as a training set of size T and produce a $(T + h)$ -step-ahead point forecast.
- 4) The process iterates from $T + 1$ to $T + H$, where the training data set with equal sample size rolls one-step-ahead each time.
- 5) With the holdout densities, we compute the point and interval forecast errors.

Since the sub-national age-specific life-table death counts can be considered a PDF, we consider some density evaluation measures to evaluate the point forecast accuracy. These metrics include

the discrete version of the Kullback-Liebler divergence (Kullback and Leibler, 1951) and the Jensen-Shannon divergence (Shannon, 1948). The Kullback-Liebler divergence is intended to measure the loss of information when we choose an approximation. For two PDFs denoted by $d_{T+h,s}^g(u)$ and $\widehat{d}_{T+h|T,s}^g(u)$, the discrete version of the Kullback-Liebler divergence is defined as

$$\text{KLD}_s^g(h) = \text{D}_{\text{KL}} \left[d_{T+h,s}^g(u_i) \parallel \widehat{d}_{T+h|T,s}^g(u_i) \right] + \text{D}_{\text{KL}} \left[\widehat{d}_{T+h|T,s}^g(u_i) \parallel d_{T+h,s}^g(u_i) \right],$$

which is symmetric and non-negative, and i represents a discretized age. An alternative is given by the Jensen-Shannon divergence defined by

$$\text{JSD}_s^g(h) = \frac{1}{2} \text{D}_{\text{KL}} \left[d_{T+h,s}^g(u_i) \parallel \delta_{T+h,s}^g(u_i) \right] + \frac{1}{2} \text{D}_{\text{KL}} \left[\widehat{d}_{T+h|T,s}^g(u_i) \parallel \delta_{T+h,s}^g(u_i) \right],$$

where $\delta_{T+h,s}^g(u_i)$ measures a common quantity between $d_{T+h,s}^g(u_i)$ and $\widehat{d}_{T+h|T,s}^g(u_i)$ (Fuglede and Topsøe, 2004). We consider geometric mean given by $\delta_{T+h,s}^g(u_i) = \sqrt{d_{T+h,s}^g(u_i) \widehat{d}_{T+h|T,s}^g(u_i)}$.

We report the averaged KLD and JSD across n_s number of states. That is,

$$\begin{aligned} \text{KLD}^g(h) &= \frac{1}{n_s \times p} \sum_{s=1}^{n_s} \sum_{i=1}^p d_{T+h,s}^g(u_i) \cdot [\ln d_{T+h,s}^g(u_i) - \ln \widehat{d}_{T+h|T,s}^g(u_i)] + \\ &\quad \frac{1}{n_s \times p} \sum_{s=1}^{n_s} \sum_{i=1}^p \widehat{d}_{T+h|T,s}^g(u_i) \cdot [\ln \widehat{d}_{T+h|T,s}^g(u_i) - \ln d_{T+h,s}^g(u_i)]. \end{aligned}$$

The average across the forecast horizons for both KLD and JSD can be computed as follows,

$$\begin{aligned} \overline{\text{KLD}}^g &= \frac{1}{H} \sum_{h=1}^H \text{KLD}^g(h) \\ \overline{\text{JSD}}^g &= \frac{1}{H} \sum_{h=1}^H \text{JSD}^g(h). \end{aligned}$$

4.1 Point forecast comparison

The results for the point forecast accuracy for the US, using the EVR criterion described in (5), are provided in Table 1. We present the KLD and JSD across the forecast horizon averaged across states and gender. We incorporate the accuracy mean over the forecast horizon. In Appendix A, we conduct additional sensitivity analysis by fixing the number of functional principal components to $K = 6$ as advocated by Hyndman et al. (2013).

Table 1: Point forecast accuracy, as measured by the KLD and JSD, for the US between the FMP-ANOVA and FM-ANOVA. All values are multiplied by a factor of 100.

h	FMP-ANOVA				FM-ANOVA			
	Female		Male		Female		Male	
	KLD	JSD	KLD	JSD	KLD	JSD	KLD	JSD
1	1.83	0.52	2.17	0.59	1.17	0.33	1.36	0.36
2	1.83	0.52	2.24	0.61	1.22	0.34	1.41	0.38
3	1.93	0.53	2.35	0.64	1.31	0.37	1.51	0.40
4	2.11	0.58	2.54	0.68	1.47	0.40	1.66	0.44
5	2.34	0.64	2.75	0.73	1.67	0.46	1.85	0.49
6	2.64	0.72	3.04	0.80	1.92	0.52	2.11	0.55
7	2.98	0.82	3.33	0.88	2.19	0.59	2.35	0.61
8	3.33	0.90	3.71	0.98	2.53	0.67	2.68	0.70
9	4.58	1.37	4.14	1.09	3.18	0.86	3.08	0.80
10	6.04	1.60	5.56	1.45	4.84	1.25	4.47	1.14
Mean	2.66	0.75	3.18	0.85	1.95	0.53	2.28	0.59

From the results in Table 1, the proposed FM-ANOVA method generally outperforms the FMP-ANOVA method. The FM-ANOVA method consistently achieves lower values for KLD and JSD. Additionally, the accuracy of point forecasts shows an increasing trend as the forecast horizon extends. When comparing the two proposed methods, the forecast errors for the female population are generally lower than that for the male population.

4.2 Competitive HDFTS forecasting methods

We discuss alternative methods from the recent HDFTS literature. For the methods introduced by Gao et al. (2019) and Tavakoli et al. (2023), we incorporate the clr transformation to ensure that the density functions belong to the same functional space during modeling and forecasting. However, the method proposed by Pascariu et al. (2019) does not require transformation, as it is designed to work directly with densities. In Appendix B, we also included the results of the two alternative methods without the clr transformation.

4.2.1 Two-stage functional principal component analysis

Gao et al. (2019) adopted a two-stage approach combining truncated principal component analysis and a separate scalar factor model for the resulting panels of scores. Their method consists of three steps.

- 1) Dynamic FPCA is performed separately on each set of functional time series, resulting in N sets of principal component scores of low dimension p_0 .
- 2) The first functional principal component scores from each of N sets of functional time series are combined into an $N \times 1$ vector. We fit factor models to the FPC scores to further reduce the dimension into an $r \times 1$ vector, where $r \ll N$. The same procedure is implemented for the second, third, and so on until the p_0^{th} FPC scores. The vector of N functional time series is reduced to an $r \times p_0$ matrix.
- 3) A scalar time series model can be fitted to each factor and forecasts are produced. The forecast factors can be used to construct forecast functions.

4.2.2 Functional factor model

For a given gender g , Tavakoli et al. (2023) introduce the following functional factor model:

$$\mathcal{X}_{st}(u) = \sum_{k=1}^{k_+} B_{sk}^+(u) F_{tk}^+ + \varepsilon_{st}(u),$$

where $B_{sk}^+(\cdot)$ is the k^{th} functional factor loading, $\mathbf{F}_t^+ = (F_{t1}^+, \dots, F_{tk_+}^+)^{\top}$ is a vector of real-valued factors, $\varepsilon_{st}(u)$ denotes the model residuals, and k_+ denotes the number of retained functional principal components.

4.2.3 Maximum entropy mortality model

In the demographic literature, several attempts exist to model the age distribution of death counts. Pascariu et al. (2019) propose matching finite (typically, the first four) statistical moments of the age distribution of death counts. The forecast life-table death counts for a population can be determined by extrapolating these moments. The extrapolation is achieved through multivariate time series models, such as multivariate random walk with drift. With the forecast moments, the forecast age distribution of death counts is then obtained.

Table 2 provides an evaluation and comparison of the point forecast accuracy for three competitive methods. In the case of the methods proposed by Tavakoli et al. (2023) and Gao et al. (2019),

the clr transformation is applied, as these methods were not originally designed for density-valued functions. To emphasize the significance of the clr transformation, we also present the point forecast results of these two methods without the transformation in Appendix B.

Table 2: Point forecast accuracy, as measured by the KLD and JSD, for the US for alternative methods TNH refers to the method of [Tavakoli et al. \(2023\)](#), GSY refers to the method of [Gao et al. \(2019\)](#), and PLC refers to the method of [Pascariu et al. \(2019\)](#). All values are multiplied by a factor of 100.

h	TNH23				GSY19				PLC19			
	Female		Male		Female		Male		Female		Male	
	KLD	JSD	KLD	JSD	KLD	JSD	KLD	JSD	KLD	JSD	KLD	JSD
1	1.00	0.28	0.93	0.25	6.84	1.77	7.58	1.90	2.38	0.52	1.89	0.66
2	1.04	0.29	1.01	0.27	8.97	2.41	9.71	2.39	2.38	0.52	1.92	0.66
3	1.10	0.30	1.15	0.31	7.68	1.96	9.60	2.50	2.42	0.55	2.02	0.67
5	1.29	0.35	1.51	0.40	7.94	2.07	9.04	2.34	2.51	0.58	2.14	0.69
5	1.21	0.33	1.34	0.36	11.53	3.24	10.68	2.76	2.57	0.62	2.31	0.71
6	1.40	0.38	1.72	0.45	9.54	2.42	8.85	2.23	2.83	0.70	2.61	0.78
7	1.54	0.42	1.97	0.51	9.18	2.32	9.38	2.34	2.91	0.75	2.84	0.79
8	1.72	0.46	2.24	0.58	14.21	3.92	10.07	2.53	3.25	0.82	3.13	0.88
9	2.02	0.54	2.64	0.69	12.46	3.13	9.42	2.36	3.72	1.00	3.80	1.01
10	2.90	0.75	3.52	0.90	12.03	3.12	11.11	2.85	4.78	1.33	5.15	1.26
Mean	1.52	0.41	1.80	0.47	10.04	2.64	9.54	2.42	2.97	0.74	2.78	0.81

Although the functional factor model introduced by [Tavakoli et al. \(2023\)](#) achieves the highest accuracy in terms of point forecasts among all the methods, the difference is not substantial when compared to our proposed FM-ANOVA.

Because of the two-stage FPCA, the method of [Gao et al. \(2019\)](#) suffers information loss and can result in the worst accuracy among the three competitors. The maximum entropy model of [Pascariu et al. \(2019\)](#) was designed for modeling the age distribution of death counts. Hinging on the existence of finite statistical moments, it provides moderate point forecast accuracy.

To gain a clearer understanding of the forecast behavior of the proposed methods in comparison to the benchmark methods, Figure 3 provides an example analysis of the life-table death count data for the state of California, segmented by gender. The first column of the figure shows the

forecast results for females, while the second column displays those for males. Each row represents a different forecast horizon, namely $h = 1, 3, 7$. From these plots, it is evident that the proposed methods effectively capture the behavior of the holdout densities, particularly for the shorter forecast horizons ($h = 1$ and $h = 3$), where the predicted trends and density shapes closely align with the observed values. However, as the forecast horizon extends to $h = 7$, we observe a noticeable decline in forecast accuracy for all methods, as anticipated, given the inherent challenges of comparably longer-term forecasting.

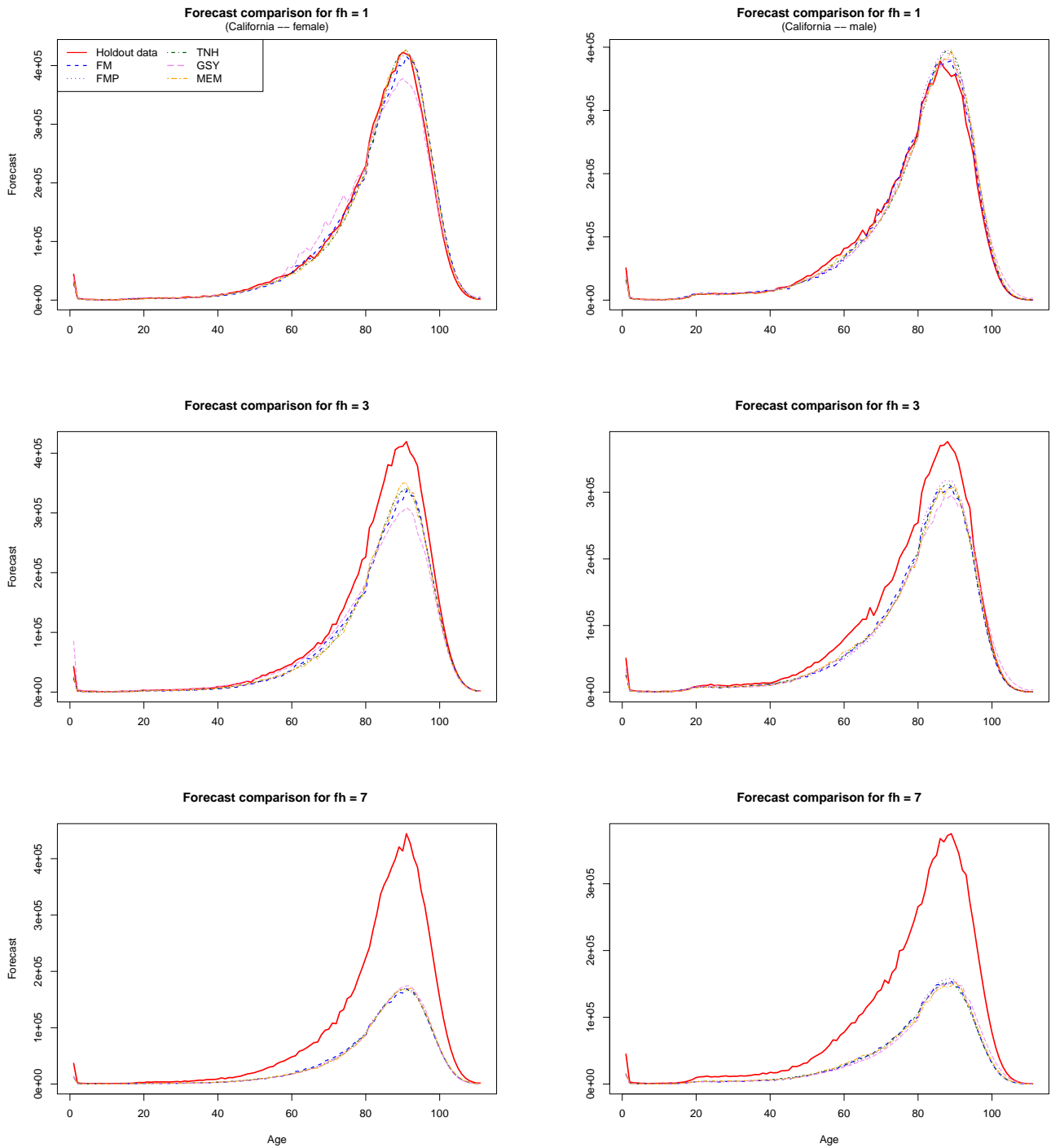


Figure 3: Comparison of plots for the female and male data in California with different horizons.

For further comparison, state- and gender-specific point forecast errors for all methods across multiple forecast horizons ($h = 1, 2, \dots, H$) can be explored interactively via the Shiny app: https://cfjimenezv.shinyapps.io/Forecasting_density_valued_functional_panel_data/.

5 Conclusion

Understanding patterns in mortality across multiple populations is essential for local health policy decision-making. By modeling life-table death counts in multiple populations at the sub-national level, we expand the clr transformation to density-valued functional panel data. We apply the clr transformation to obtain unconstrained functional panel data. The time-varying components in the functional panel data are then obtained using two-way functional ANOVA decomposition across several states and genders. In the unconstrained space, we apply a functional time series method to forecast the time-varying component. Using the inverse clr transformation, we obtain forecasts for the age-specific life-table death counts for multiple populations. The estimate of subpopulation mortality risks is needed to identify and understand the mortality patterns of vulnerable groups and track the effects of policy responses.

Within the clr transformation, we introduce the FMP-ANOVA and FM-ANOVA decompositions for density-valued functional panel data. Both approaches provide a decomposition to decompose the original HDFTS into deterministic and time-varying components within an unrestricted domain. We demonstrate that incorporating the clr transformation improves the forecast accuracy.

The paper could be expanded in several ways, and we briefly mention three. 1) The HDFTS could also be extended beyond gender and state-specific populations in this research. Future extensions may include various subsets within each population (e.g., by socioeconomic class, ethnic group, or education level). 2) In the case of outlying years, a robust clr transformation, such as that proposed by [Filzmoser et al. \(2009\)](#), may be used. 3) We outline as future work the development of uniform prediction bands and the assessment of empirical coverage probability difference for the life table death counts considered as densities.

Supplementary Materials

 **code for functional time series forecasting based on FMP-ANOVA and FM-ANOVA within the clr transformation.** Producing point forecasts from the two approaches described in the paper, including the clr transformation. The R codes are available at the following repository:

https://github.com/cfjimenezv07/CoDa_life_table_death_counts

 **code for shiny application.** Producing a shiny user interface for plotting every series and the results for point for the US life-table death count database. The R codes are available at the following repository: https://github.com/cfjimenezv07/CoDa_life_table_death_counts

Acknowledgement

We are grateful to the FDA workshop participants in Lille, France and the participants in the EcoSta2024 conference in Beijing, China. The first author thanks the financial support from King Abdullah University of Science and Technology. The third author thanks fundings from Macquarie University Data Horizons consilience center, the Australian Research Council Discovery Project DP230102250 and Future Fellowship FT240100338.

References

- Aburto, J. M., U. Basellini, A. Baudisch, and F. Villavicencio (2022). Drownowski's index to measure lifespan variation: Revisiting the Gini coefficient of the life table. *Theoretical Population Biology* 148, 1–10.
- Ahn, S. C. and A. R. Horenstein (2013). Eigenvalue ratio test for the number of factors. *Econometrica* 81(3), 1203–1227.
- Aitchison, J. (1982). The statistical analysis of compositional data. *Journal of the Royal Statistical Society. Series B (Methodological)* 44(2), 139–177.
- Basellini, U., C. G. Camarda, and H. Booth (2023). Thirty years on: A review of the Lee–Carter method for forecasting mortality. *International Journal of Forecasting* 39(3), 1033–1049.
- Basellini, U., S. Kjærgaard, and C. G. Camarda (2020). An age-at-death distribution approach to forecast cohort mortality. *Insurance: Mathematics and Economics* 91(C), 129–143.
- Bergeron-Boucher, M.-P., V. Canudas-Romo, J. Oeppen, and J. W. Vaupel (2017). Coherent forecasts of mortality with compositional data analysis. *Demographic Research* 37, 527–566.
- Brouhns, N., M. Denuit, and J. K. Vermunt (2002). Measuring the longevity risk in mortality projections. *Bulletin of the Swiss Association of Actuaries* 2, 105–130.
- Canudas-Romo, V. (2010). Three measures of longevity: Time trends and record values. *Demography* 47(2), 299–312.
- Chang, J., C. Chen, X. Qiao, and Q. Yao (2024). An autocovariance-based learning framework for high-dimensional functional time series. *Journal of Econometrics* 239(2), 105385.
- Chang, J., Q. Fang, X. Qiao, and Q. Yao (2025). On the modelling and prediction of high-dimensional functional time series. *Journal of the American Statistical Association: Theory and Methods* in press.
- Chang, Y., C. S. Kim, and J. Y. Park (2016). Nonstationarity in time series of state densities. *Journal of Econometrics* 192(1), 152–167.
- Chiou, J.-M. (2012). Dynamical functional prediction and classification with application to traffic flow prediction. *The Annals of Applied Statistics* 6(4), 1588–1614.

- Condino, F. (2023). Share density-based clustering of income data. *Statistical Analysis and Data Mining* 16, 336–347.
- Filzmoser, P., K. Hron, and C. Reimann (2009). Principal component analysis for compositional data with outliers. *Environmetrics* 20(6), 621–632.
- Fuglede, B. and F. Topsøe (2004). Jensen-Shannon divergence and Hilbert space embedding. In *International Symposium on Information Theory*, pp. 30.
- Gao, Y., H. L. Shang, and Y. Yang (2019). High-dimensional functional time series forecasting: An application to age-specific mortality rates. *Journal of Multivariate Analysis* 170, 232–243.
- Guo, S. and X. Qiao (2023). On consistency and sparsity for high-dimensional functional time series with application to autoregressions. *Bernoulli* 29(1), 451–472.
- Guo, S., X. Qiao, Q. Wang, and Z. Wang (2024). Factor modelling for high-dimensional functional time series. Working paper, arXiv. URL: <https://arxiv.org/abs/2112.13651>.
- Hall, P. and C. Vial (2006). Assessing the finite dimensionality of functional data. *Journal of the Royal Statistical Society: Series B* 68(4), 689–705.
- Hallin, M., G. Nisol, and S. Tavakoli (2023). Factor models for high-dimensional functional time series I: Representation results. *Journal of Time Series Analysis* 44(5-6), 578–600.
- Horta, E. and F. Ziegelmann (2018). Dynamics of financial returns densities: A functional approach applied to the Bovespa intraday index. *International Journal of Forecasting* 34, 75–88.
- Horváth, L., G. Rice, and S. Whipple (2016). Adaptive bandwidth selection in the long run covariance estimator of functional time series. *Computational Statistics and Data Analysis* 100, 676–693.
- Hron, K., A. Menafoglio, M. Templ, K. Hružová, and P. Filzmoser (2016). Simplicial principal component analysis for density functions in Bayes space. *Computational Statistics & Data Analysis* 94, 330–350.
- Human Mortality Database (2024). *Max Planck Institute for Demographic Research (Germany), University of California, Berkeley (USA), and French Institute for Demographic Studies (France)*. Available at www.mortality.org. (data downloaded on June 14, 2023).

- Hyndman, R. J., H. Booth, and F. Yasmeen (2013). Coherent mortality forecasting: the product-ratio method with functional time series models. *Demography* 50(1), 261–283.
- Hyndman, R. J. and Y. Khandakar (2008). Automatic time series forecasting: the forecast package for R. *Journal of Statistical Software* 27(3), 1–22.
- Jiménez-Varón, C. F., Y. Sun, and H. L. Shang (2024). Forecasting high-dimensional functional time series: Application to sub-national age-specific mortality. *Journal of Computational and Graphical Statistics* 33(4), 1160–1174.
- Kullback, S. and R. A. Leibler (1951). On information and sufficiency. *The Annals of Mathematical Statistics* 22(1), 79–86.
- Kwiatkowski, D., P. C. Phillips, P. Schmidt, and Y. Shin (1992). Testing the null hypothesis of stationarity against the alternative of a unit root: How sure are we that economic time series have a unit root? *Journal of Econometrics* 54(1), 159–178.
- Li, D., R. Li, and H. L. Shang (2024). Detection and estimation of structural breaks in high-dimensional functional time series. *The Annals of Statistics* 52, 1716–1740.
- Li, D., P. M. Robinson, and H. L. Shang (2020). Long-range dependent curve time series. *Journal of the American Statistical Association: Theory and Methods* 115, 957–971.
- Li, D., P. M. Robinson, and H. L. Shang (2021). Local Whittle estimation of long-range dependence for functional time series. *Journal of Time Series Analysis* 42(5-6), 685–695.
- Mercer, J. and A. R. Forsyth (1909). Xvi. functions of positive and negative type, and their connection the theory of integral equations. *Philosophical Transactions of the Royal Society of London. Series A, Containing Papers of a Mathematical or Physical Character* 209(441-458), 415–446.
- Oeppen, J. (2008). Coherent forecasting of multiple-decrement life tables: A test using Japanese cause of death data. In *European Population Conference*. European Association for Population Studies. URL: <https://epc2008.eaps.nl/papers/80611>.
- Pascariu, M. D., A. Lenart, and V. Canudas-Romo (2019). The maximum entropy mortality model: Forecasting mortality using statistical moments. *Scandinavian Actuarial Journal* 2019(8), 661–685.
- Ramsay, J. and B. Silverman (2006). *Functional Data Analysis*. Springer Series in Statistics. New York: Springer.

- Rice, G. and H. L. Shang (2017). A plug-in bandwidth selection procedure for long-run covariance estimation with stationary functional time series. *Journal of Time Series Analysis* 38(4), 591–609.
- Robine, J.-M. (2001). Redefining the stages of the epidemiological transition by a study of the dispersion of life spans: the case of France. *Population: An English Selection* 13(1), 173–193.
- Scealy, J. L., P. de Caritat, E. C. Grunsky, M. T. Tsagris, and A. H. Welsh (2015). Robust principal component analysis for power transformed compositional data. *Journal of the American Statistical Association: Applications and Case Studies* 110(509), 136–148.
- Scealy, J. L. and A. H. Welsh (2017). A directional mixed effects model for compositional expenditure data. *Journal of the American Statistical Association: Applications and Case Studies* 112(517), 24–36.
- Seo, W.-K. and B. K. Beare (2019). Cointegrated linear processes in Bayes Hilbert space. *Statistics & Probability Letters* 147, 90–95.
- Shang, H. L. (2019). Dynamic principal component regression: Application to age-specific mortality forecasting. *ASTIN Bulletin* 49(3), 619–645.
- Shang, H. L. and S. Haberman (2020). Forecasting age distribution of death counts: An application to annuity pricing. *Annals of Actuarial Science* 14(1), 150–169.
- Shang, H. L., S. Haberman, and R. Xu (2022). Multi-population modelling and forecasting life-table death counts. *Insurance: Mathematics and Economics* 106, 239–253.
- Shang, H. L. and F. Kearney (2022). Dynamic functional time-series forecasts of foreign exchange implied volatility surfaces. *International Journal of Forecasting* 38(3), 1025–1049.
- Shannon, C. E. (1948). A mathematical theory of communication. *Bell System Technical Journal* 27(3), 379–423.
- Sun, Y. and M. G. Genton (2012). Functional median polish. *Journal of Agricultural, Biological, and Environmental Statistics* 17(3), 354–376.
- Tan, J., D. Liang, Y. Guan, and H. Huang (2024). Graphical principal component analysis of multivariate functional time series. *Journal of the American Statistical Association: Theory and Methods* 119, 3073–3085.

- Tang, C., H. L. Shang, and Y. Yang (2022). Clustering and forecasting multiple functional time series. *The Annals of Applied Statistics* 16(4), 2523–2553.
- Tavakoli, S., G. Nisol, and M. Hallin (2023). Factor models for high-dimensional functional time series II: Estimation and forecasting. *Journal of Time Series Analysis* 44(5-6), 601–621.
- Tukey, J. (1977). *Exploratory Data Analysis*. Reading: Addison-Wesley.
- United States Mortality Database (2024). *University of California, Berkeley (USA)*. Department of Demography at the University of California, Berkeley. Available at usa.mortality.org (data downloaded on March 15, 2023).
- Yao, F., H.-G. Müller, and J.-L. Wang (2005). Functional data analysis for sparse longitudinal data. *Journal of the American Statistical Association: Theory and Methods* 100(470), 577–590.
- Zhang, J.-T. (2014). *Analysis of Variance for Functional Data*. Boca Raton: Chapman & Hall/CRC.
- Zhang, Q., A. Makur, and K. Azizzadenesheli (2024). Functional linear regression of cumulative distribution functions. Working paper, arXiv. URL: <https://arxiv.org/abs/2205.14545>.
- Zhou, Z. and H. Dette (2023). Statistical inference for high-dimensional panel functional time series. *Journal of the Royal Statistical Society Series B: Statistical Methodology* 85(2), 523–549.
- Zivot, E. and J. Wang (2006). *Modeling Financial Time Series with S-PLUS*. New York: Springer.

A Number of functional principal components $K = 6$

We conducted an additional analysis by fixing the number of retained components at $K = 6$, as it has been shown that this number of components is enough for forecasting (Hyndman et al., 2013).

Table 3 presents the results regarding the point forecast errors.

Table 3: With $K = 6$, point forecast accuracy, as measured by the KLD and JSD, for the US between the FMP-ANOVA and FM-ANOVA. All values are multiplied by a factor of 100.

h	FMP-ANOVA				FM-ANOVA			
	Female		Male		Female		Male	
	KLD	JSD	KLD	JSD	KLD	JSD	KLD	JSD
1	2.08	0.62	2.10	0.59	1.18	0.34	1.27	0.34
2	2.02	0.60	2.11	0.58	1.16	0.33	1.34	0.36
3	2.04	0.59	2.29	0.62	1.25	0.35	1.50	0.40
4	2.13	0.61	2.50	0.67	1.39	0.39	1.67	0.44
5	2.30	0.66	2.71	0.72	1.55	0.43	1.86	0.49
6	2.53	0.72	3.03	0.80	1.78	0.49	2.13	0.55
7	2.67	0.75	3.35	0.89	1.97	0.53	2.39	0.62
8	2.91	0.80	3.74	0.99	2.26	0.61	2.75	0.71
9	3.40	0.93	4.30	1.13	2.89	0.79	3.26	0.84
10	4.53	1.20	5.72	1.49	4.07	1.05	4.58	1.17
Mean	2.96	0.82	3.18	0.84	2.15	0.58	2.25	0.59

B Alternative methods without the clr transformation

Table 4 displays the point forecast error results for two competitive methods: TNH by [Tavakoli et al. \(2023\)](#) and GSY by [Gao et al. \(2019\)](#). When these methods are directly applied, the generated functional curves may not belong to the functional space where the densities are located. Consequently, any negative values in the forecasts were set to zero, and the forecasts were subsequently normalized to 10^5 .

Table 4: Point forecast accuracy, as measured by the KLD and JSD, for the US for alternative methods without the clr transformation. TNH refers to the method of [Tavakoli et al. \(2023\)](#), GSY refers to the method of [Gao et al. \(2019\)](#). All values are multiplied by a factor of 100.

<i>h</i>	TNH23				GSY19			
	Female		Male		Female		Male	
	KLD	JSD	KLD	JSD	KLD	JSD	KLD	JSD
1	10.66	3.13	11.67	3.49	5.22	1.53	5.53	1.55
2	10.68	3.14	11.74	3.52	5.99	1.77	5.47	1.53
3	10.98	3.23	11.84	3.54	6.67	1.99	5.57	1.54
4	11.33	3.33	11.87	3.55	6.12	1.82	6.59	1.81
5	11.61	3.41	11.91	3.57	6.50	1.92	7.69	2.18
6	12.09	3.56	11.94	3.58	8.03	2.41	7.95	2.23
7	12.70	3.74	12.08	3.62	7.54	2.25	8.84	2.46
8	13.39	3.95	12.32	3.70	8.27	2.46	11.23	3.23
9	14.05	4.16	13.01	3.93	8.97	2.66	9.49	2.75
10	15.40	4.60	14.58	4.45	10.89	3.26	19.44	5.91
Mean	12.29	3.63	12.30	3.70	7.42	2.21	8.78	2.52